Surface Reactions of CH_3I and CF_3I with Coadsorbed CH_2I_2 on Ag(111) as Mechanistic Probes for Carbon−Carbon Bond Formation via Methylene Insertion

Hsiao-Jung Wu, Heng-Kai Hsu,† and Chao-Ming Chiang*

Contribution from the Department of Chemistry, National Sun Yat-Sen University, Kaohsiung, Taiwan 80424

Received September 3, 1998

Abstract: The insertion of methylene into metal−alkyl bonds has been studied on an Ag(111) surface under ultrahigh-vacuum conditions. Methyl (CH_3) and methylene (CH_2) groups are generated on Ag(111) by thermal scission of the C−I bonds in adsorbed methyl iodide (CH_3I) and methylene iodide (CH_2I_2) below 200 K. When studying the bimolecular interaction of coadsorbed CH_3 and CH_2 moieties, *propane* and *butane* are detected in the temperature-programmed reaction (TPR) experiments, suggesting that CH_2 inserts into the Ag−CH_3 bond to produce metal-bound *ethyl* (CH_2CH_3) groups, followed by facile self-/cross-coupling of existing alkyl groups on the surface. In a separate approach, CF_3 is used instead of CH_3 as the target for CH_2 insertion. TPR studies of the coadsorbed CF_3 and CD_2 show that CD_2 also inserts into the Ag−CF_3 bond to form a new C−C bond; however, a different chain termination step (β-fluoride elimination) is observed to produce 1,1-difluoroethylene-d_2 (CF_2═CD_2) in the gas phase. Two sequential methylene insertions are also implicated, as evidenced by the production of 1,1,1-trifluoropropyl iodide-2,3-d_4 ($CF_3CD_2CD_2I$) as a result of the recombination of $CF_3CD_2CD_2$ groups with surface iodine. The relative rates of methylene insertion, alkyl coupling, and β-elimination involved in the reaction mechanisms are systematically compared. The effect of coadsorbed iodine on the reaction pathways is assessed. The methylene insertion rate is found to be more facile on silver than on copper surfaces.

1. Introduction

The formation of carbon−carbon bonds catalyzed by either transition-metal complexes or surfaces is a central and challenging subject in both organometallic chemistry[1] and surface science.[2] Among various C−C bond-forming processes, such as *reductive elimination* from alkyls[3] and metallacycles as well as *migratory insertion* of carbenes and olefins, the insertion of carbene (methylene) into metal−alkyl bonds is recognized as a key reaction in some heterogeneous catalytic processes[4] and in many homogeneous catalytic transformations.[5] The impetus for research in this area is that this reaction can, in principle, proceed in a catalytic cycle to produce polymers. Thus, it is of great interest to determine the chemical requirements for causing such a reaction and to understand its mechanism. One common approach to unravel the mechanisms of catalytic reactions is to judiciously choose molecular precursors which can thermally dissociate on the transition-metal surface of interest to isolate the desired key intermediates as model systems. Many systems, including alkyls, vinyl, allyl, aryl, and methylene,[6] have been thoroughly investigated. With the aid of modern surface analysis techniques, one can then characterize the elementary steps involved in the catalytic processes. While there are many good examples using this methodology to probe the mechanistic details concerning metal-assisted bond activation and formation, there have been fewer cases which delve into the C−C bond-forming reaction via migratory insertion of methylene (CH_2) into metal−alkyl bonds.

On a more practical level, sequential methylene insertions are thought to be responsible for converting the incipient surface-bound C_1 species into a distribution of longer-chain hydrocarbons under real catalytic Fischer−Tropsch conditions. Understanding the methylene insertion reaction should help in developing methods (better catalysts) for transforming coal to gasoline. In a previous communication,[7] we reported our discovery of CH_2 insertion into the Ag−CF_3 bond, utilizing methylene iodide (CH_2I_2) and trifluoromethyl iodide (CF_3I) as precursors for preparing coadsorbed methylene and perfluoromethyl fragments. As a consequence, we were able to demonstrate that the Ag(111) surface catalyzes the formation of a new C−C bond between these two C_1 moieties via the CH_2 insertion reaction. Here we use temperature-programmed reaction spectroscopy (TPRS) to study the bimolecular interactions of metal-bound *methyl* and *perfluoromethyl* in conjunction with coadsorbed methylene. In both cases, the desorbing products are unique enough to demand unequivocally the

* To whom correspondence should be directed. Phone: 886-7-525-3939. Fax: 886-7-525-3908. E-mail: cmc@mail.nsysu.edu.tw.

† Present address: ProMos Technologies Inc., Hsinchu, Taiwan.

(1) Hegedus, L. S. In *Comprehensive Organometallic Chemistry II*; Abel, E. W., Stone, F. G. A., Wilkinson, G., Eds.; Pergamon: Oxford, U.K., 1995; Vol. 12.

(2) For an outstanding review, see: Zaera, F. *Chem. Rev.* **1995**, *95*, 2651.

(3) Paul, A.; Bent, B. E. *J. Catal.* **1994**, *147*, 264.

(4) (a) Maitlis, P. M.; Long, H. C.; Quyoum, R.; Turner, M. L.; Wang, Z.-Q. *J. Chem. Soc., Chem. Commun.* **1996**, 1. (b) Brady, R. C., III; Pettit, R. *J. Am. Chem. Soc.* **1980**, *102*, 6181 and references therein.

(5) (a) Saez, I. M.; Meanwell, N. J.; Nutton, A.; Isobe, K.; de Miguel, A. M.; Bruce, D. W.; Okeya, S.; Andrews, D. G.; Ashton, P. R.; Johnstone, I. R.; Maitlis. P. M. *J. Chem. Soc., Dalton Trans.* **1986**, 1565. (b) Thorn, D. L.; Tulip, T. H. *J. Am. Chem. Soc.* **1981**, *103*, 5984 and references therein.

(6) For an excellent review on this approach, see: Bent, B. E. *Chem. Rev.* **1996**, *96*, 1361.

(7) Wu, H.-J.; Chiang, C.-M. *J. Phys. Chem.* **1998**, *102*, 7075.

10.1021/ja983164c CCC: $18.00
Published on Web 04/24/1999

participation of the methylene insertion reaction. The mechanisms also involve the intricate interplay of several basic organometallic reactions, including oxidative addition, reductive coupling, methylene insertion, and β-elimination. The different rates of these elementary steps determine the propagation and termination of the carbon chains.

2. Experimental Section

All experiments were performed in a stainless steel ultrahigh-vacuum (UHV) chamber evacuated by a turbomolecular pump (Varian, 250 L/s), backed by combined oil-free molecular-drag and diaphragm pumps (Alcatel Drytel 31) to a base pressure of 2×10^{-10} Torr. The chamber is equipped with a sputter-cleaning ion source (Omicron ISE10) and a retarding field analyzer (Omicron SPECTALEED) for both Auger electron spectroscopy (AES) and low-energy electron diffraction (LEED). It also contains a mass spectrometer (Hiden, 510 amu) for residual gas analysis and detection of gas-phase products during temperature-programmed reaction/desorption (TPR/D) measurements. The quadrupole head of the mass spectrometer is covered by an ion-pumped stainless steel housing with a 2-mm-diameter aperture for sampling molecules evolving from the central region of the crystal surface during TPR/D studies. Gas dosing was accomplished through a 0.76-mm-i.d. stainless steel tube that is connected to a precision leak valve, and there are two sets of this dosing apparatus for handling two different gas samples.

The disk-shaped Ag(111) crystal (10 mm in diameter, 2 mm thick, 5 N purity from Monocrystals) was first manually polished to a mirror finish by using alumina grits (in 1, 0.3, and 0.05 μm order) and then placed within the UHV system. The crystal was mounted on a molybdenum plate with four clips. Heating was achieved through radiation from a hot tungsten filament located at the back of the molybdenum plate. Active cooling was executed by feeding liquid nitrogen through a coil of stainless steel tubing into an OFHC copper block, to which the molybdenum plate is attached. With this mounting scheme, sample temperatures could be controlled from 100 to 1200 K and were measured by a chromel−alumel thermocouple (0.127 mm) whose junction was wedged into a hole on the edge of the crystal. It is often desirable to maintain a constant crystal temperature for a long period of time or to heat the crystal at a reproducible rate. To meet these requirements, a commercial temperature controller (Eurotherm 818P) was used. It consists of a programmable proportional-integral-differential (PID) feedback circuit coupled to a dc power supply to regulate the heating of the tungsten filament mentioned above. After pump-down and bake-out of the chamber, the Ag(111) surface was cleaned by 3−4 cycles of Ar^+ sputtering at room temperature for 30 min and at 900 K for 5 min. The Ar^+ beam voltage and current to the sample were typically 1 keV and 5−6 μA, respectively. The oxygen, carbon, and sulfur impurities could be removed from the surface, and surface cleanliness before and after experiments was measured by AES. Surface order was recovered by annealing the sample to 950 K for 5 min and verified by LEED.

Diiodomethane (CH_2I_2), diiodomethane-d_2 (CD_2I_2), iodomethane (CH_3I), iodoethane (C_2H_5I), iodopropane (C_3H_7I), and 1,1,1-trifluoroethyl iodide (CF_3CH_2I) were all 99% purity and were obtained from Aldrich. 1,1,1-Trifluoropropyl iodide ($CF_3CH_2CH_2I$, 99.0% purity) was purchased from Lancaster Synthesis. All the above liquid compounds are light sensitive, and they were initially filtered through a column of basic alumina to remove acidic HI and I_2 formed as a result of photochemical degradation. The liquid compound was transferred to a glass ampule, which was attached to a bakeable, stainless steel gas-handling manifold via a glass-to-kovar seal. Several freeze−pump−thaw cycles were performed under vacuum (10^{-6} Torr) before introduction of the samples into the UHV system. Trifluoromethyl iodide (CF_3I, 99%, Aldrich), a gaseous compound, was used without additional purification. The purity of the dosing gases was confirmed in situ by mass spectrometry.

Prior to each TPR experiment, the single-crystal surface was exposed to gaseous reactants at 110 K by positioning the sample front approximately 3 cm from the doser. The pressure of the adsorbate in the chamber, as measured by the ion gauge in this dosing geometry, multiplied by the dosing time constituted our measurement of the exposure, which was given in langmuirs (L), where $1\ L = 1 \times 10^{-6}$ Torr·s. The pressure readings were not corrected for differences in ion gauge sensitivities of the compounds. The adsorbate-covered surface was positioned line-of-sight to the mass spectrometer, about 1 cm away from the sampling aperture, and could be heated at variable rates ranging from 0.5 to 5 K/s. The ion intensities (up to 20 ions simultaneously) and thermocouple readings were both interfaced to a personal computer for data acquisition and storage. All mass scan and TPR spectra were taken with the mass spectrometer ionizer energy set at 70 eV.

3. Results and Interpretation

The conceptual idea is to use surface-bound CH_3 or CF_3 as one species and CH_2 as a coadsorbate. By themselves, these three species either recombine (carbon−carbon coupling) or desorb as radicals (metal−carbon homolysis). When they are mixed, we hope to see their mutual interaction provoking the desired migratory insertion of CH_2 into the metal−carbon bond. The chemistry of the individual species is investigated first, followed by the chemistry of coadsorbed mixtures to reveal their differences and implications.

3.1. The Chemistry of CH_3I. The reactivity of alkyl halides on metal surfaces has become a subject of interest in recent years because of the ease with which these halides dissociate upon thermal activation to generate alkyl fragments. On Ag(111), alkyl groups undergo C−C coupling to form alkanes of twice the chain length. These coupling reactions have been well documented by White and co-workers.[8−11] In good agreement with their findings, our studies of CH_3I, C_2H_5I, and C_3H_7I on the Ag(111) surface also show the evolution of CH_3CH_3, $CH_3(CH_2)_2CH_3$, and $CH_3(CH_2)_4CH_3$ as the sole reaction products, respectively. Specifically, from the TPR spectra in Figure 1, the desorption features of $m/e = 142$ (CH_3I^+) and 127 (I^+, the cracking of CH_3I due to ionization in the mass spectrometer) at 130 and 210 K represent the physisorbed multilayer and monolayer CH_3I, respectively. The fragmentation pattern based on $m/e = 30$, 29, 27, and 26 signals at 255 K confirms the formation and desorption of ethane as it closely matches the data in the mass spectral handbook.[12]

The observation of CH_3I and C_2H_6 from a monolayer coverage (~0.8 L) indicates that CH_3I undergoes both molecular desorption and dissociation. A fraction of adsorbed CH_3I (~35%[7]) dissociates below 200 K to form methyl groups $CH_{3(ad)}$ and $I_{(ad)}$. This process of carbon−halogen bond scission is known as oxidative addition, which is a common route to metal−alkyl compounds.[13,14] The adsorbed methyl groups then undergo reductive elimination (C−C coupling) to produce ethane even below room temperature. In terms of the fate of iodine, studies of halogens adsorbed on other metals showed that they usually desorb either in atomic form or as metal halides.[11] In our studies, we were unable to detect any I_2 ($m/e = 254$) or AgI (as monitored by $m/e = 107$ and 109) from Ag(111). Therefore, the iodine present on the surface due to C−I bond dissociation probably desorbs as atoms above 700 K. No

(8) Zhou, X.-L.; Solymosi, F.; Blass, P. M.; Cannon, K. C.; White, J. M. *Surf. Sci.* **1989**, *219*, 294.
(9) Zhou, X.-L.; White, J. M. *Catal. Lett.* **1989**, *2*, 375.
(10) Zhou, X.-L.; Castro, M. E.; White, J. M. *Surf. Sci.* **1990**, *238*, 215.
(11) Zhou, X.-L.; White, J. M. *J. Phys. Chem.* **1991**, *95*, 5575.
(12) McLafferty F. W.; Stauffer, D. B. *The Wiley/NBS Registry of Mass Spectral Data*; Wiley: New York, 1989.
(13) Collman, J. P.; Hegedus, L. S.; Norton, J. R.; Finke, R. G. *Principles and Applications of Organotransition Metal Chemistry*; University Science Books: Mill Valley, CA, 1987.
(14) Zaera, F. *Acc. Chem. Res.* **1992**, *25*, 260.

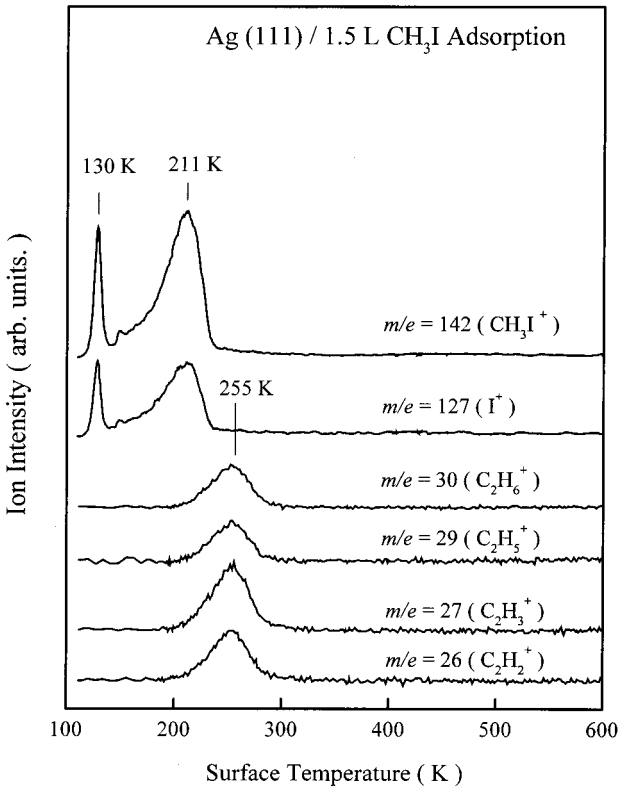

Figure 1. TPR spectra of CH_3I adsorbed on Ag(111). The peaks at 130 and 211 K for $m/e = 142$ (CH_3I^+) and 127 (I^+) reflect molecular desorption from the mulitilayer and monolayer, respectively. The traces of $m/e = 30$ ($C_2H_6^+$), 29 ($C_2H_5^+$), 27 ($C_2H_3^+$), and 26 ($C_2H_4^+$) indicate that the chemisorbed CH_3I on Ag(111) at 110 K dissociates to $CH_{3(ad)}$ and $I_{(ad)}$ during TPR. $CH_{3(ad)}$ recombines around 255 K to produce $C_2H_{6(g)}$.

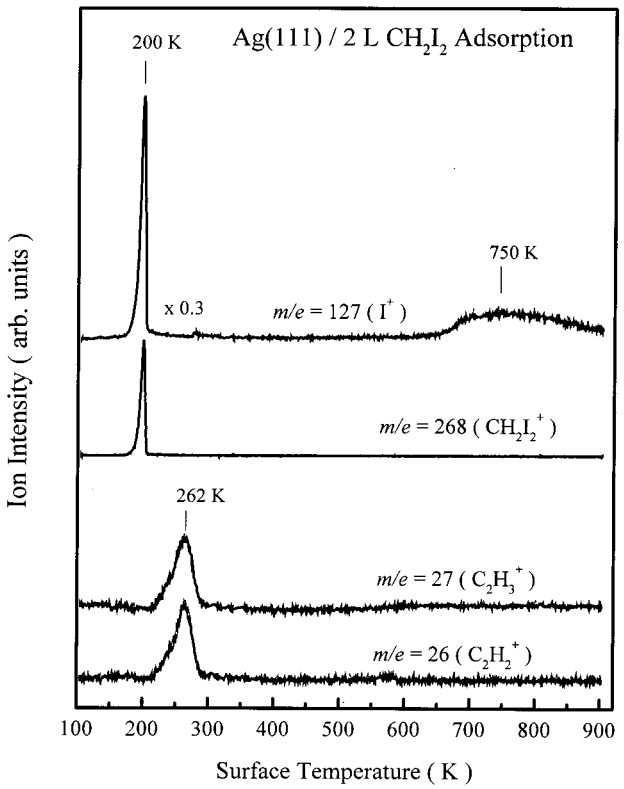

Figure 2. TPR spectra of $m/e = 268$ ($CH_2I_2^+$), 127 (I^+), 27 ($C_2H_3^+$), and 26 ($C_2H_2^+$) after a 2 L exposure of CH_2I_2 to Ag(111) at 110 K. The integrated ion intensity ratio of m/e 27 to 26 is 0.93, confirming that the product is ethylene (C_2H_4). The heating rate in this TPR experiment is 1.25 K/s.

evidence for C−H bond cleavage was observed in the TPR experiments.

3.2. The Chemistry of CH_2I_2. The dominant reaction of methylene is believed to be the insertion into available bonds. There is experimental[15] and theoretical[16] evidence that methylene inserts into H−H and C−H bonds with no energy barrier. The role of methylene (CH_2), via its insertion into metal−carbon bonds, is thought to be that of the active chain growth species in the Fischer−Tropsch synthesis.[4,17] Although definitive spectroscopic verification is always difficult to obtain, quite a number of molecular precursors have been investigated to isolate and identify this species on metal surfaces.[6] In particular, diiodomethane (CH_2I_2) has been demonstrated as a source of adsorbed methylene (CH_2) on a variety of metal surfaces by several research groups.[18−23] Here we present experimental results regarding the surface chemistry of CH_2I_2 on clean Ag(111), and the generation of surface-bound methylene moieties is implicated.

Figure 2 shows the TPR results after adsorbing 2 L diiodomethane (CH_2I_2) on the clean Ag(111) surface at 110 K. The TPR/D survey indicates that the desorbing products are molecular diiodomethane, ethylene, and iodine. CH_2I_2 desorbs molecularly from the surface at 200 K based on features of $m/e = 268$ ($CH_2I_2^+$) and 127 (I^+, the cracking of CH_2I_2 by the ionizer of the mass spectrometer). Both $m/e = 26$ ($C_2H_2^+$) and 27 ($C_2H_3^+$) ion signals, indicative of a two-carbon species, display peaks bearing the same shape and a maximum temperature at ∼260 K. The integrated intensity ratio of $m/e = 26$−27 is ∼0.9, consistent with the fragmentation pattern of ethylene (C_2H_4).[12] This observation implies that some fractions of CH_2I_2 dissociatively adsorb at submonolayer coverages on Ag(111). On the basis of the low-temperature C−I bond scission in iodomethane, we assume that $CH_{2(ad)}$ is generated below 200 K when CH_2I_2 is adsorbed on the surface. This assumption is supported by the studies of CH_2I_2 adsorbed on an Ag film and an Ag(110) surface by Domen and Chuang,[24] claiming that there is significant (20%−30%) thermal decomposition of the molecule even at around 130 K. The presence of surface methylene moieties is further substantiated by the C_2H_4 evolution attributable to direct $CH_{2(ad)}$ coupling. Since weakly chemisorbed molecular C_2H_4 desorbs at ∼140 K on clean Ag(111),[11] the evolution of C_2H_4 at 260 K must be surface reaction limited.

The coverage-dependent study of ethylene formation is followed by monitoring the signals of $m/e = 27$ shown in Figure 3. The peak becomes observable after 0.05 L exposure of CH_2I_2. The integrated areas of this peak increase with ascending

(15) (a) Jones, M.; Moss, R. A. *Carbene*; Wiley: New York, 1792 (Vol. 1) and 1975 (Vol. 2). (b) Kirmse, W. *Carbene Chemistry*; Academic: New York, 1971.

(16) (a) Bauschlicher, C. W.; Haber, K.; Schaefer, H. F., III; Bender, C. F. *J. Am. Chem. Soc.* **1977**, *99*, 3610. (b) Kollmar, H. *J. Am. Chem. Soc.* **1978**, *100*, 2660.

(17) (a) Blyholder, G.; Emmet, P. H. *J. Phys. Chem.* **1959**, *63*, 962; *J. Phys. Chem.* **1959**, *64*, 470. (b) Brock, H.; Tschmutowa, G.; Wolf, H. P. *J. Chem. Soc., Chem. Commun.* **1986**, 1068.

(18) Domen, K.; Chuang, T. J. *J. Am. Chem. Soc.* **1987**, *109*, 5288.

(19) Chiang, C.-M.; Wentzlaff, T. H.; Jenks, C. J.; Bent, B. E. *J. Vac. Sci. Technol. A* **1992**, *10*, 2185.

(20) Tjandra, S.; Zaera, F. *J. Catal.* **1993**, *144*, 361.

(21) Weldon, M. K.; Friend, C. M. *Surf. Sci.* **1994**, *321*, L202.

(22) Imre, K.; Solymosi, F. *J. Phys. Chem. B* **1997**, *101*, 5397.

(23) Wu, G.; Bartlett, B. F.; Tysoe, W. T. *Surf. Sci.* **1997**, *373*, 129.

(24) Domen, K.; Chuang, T. J. *J. Chem. Phys.* **1989**, *90*, 3332.

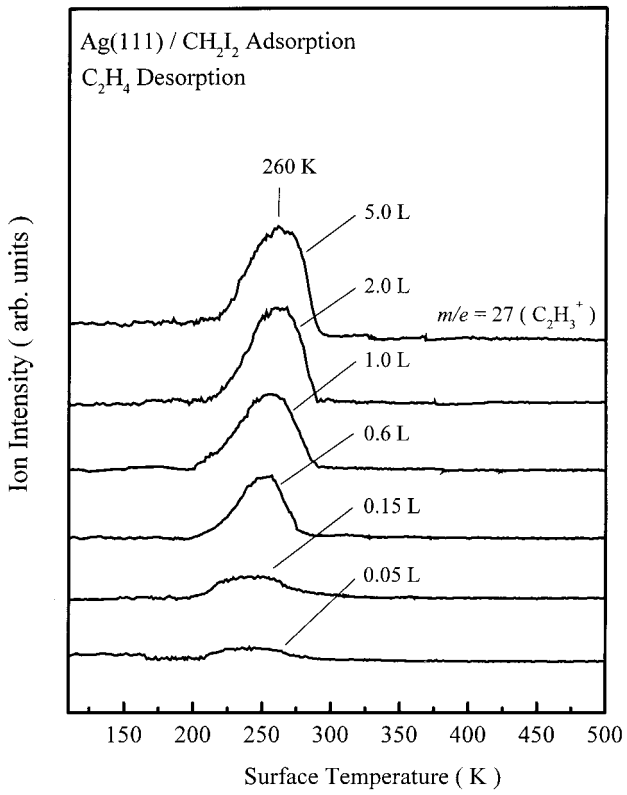

Figure 3. TPR spectra of $m/e = 27$ (predominantly $C_2H_3^+$ from C_2H_4) as a function of CH_2I_2 exposure: 0.05, 0.15, 0.6, 1.0, 2.0, and 5.0 L. The heating rate is 1.25 K/s.

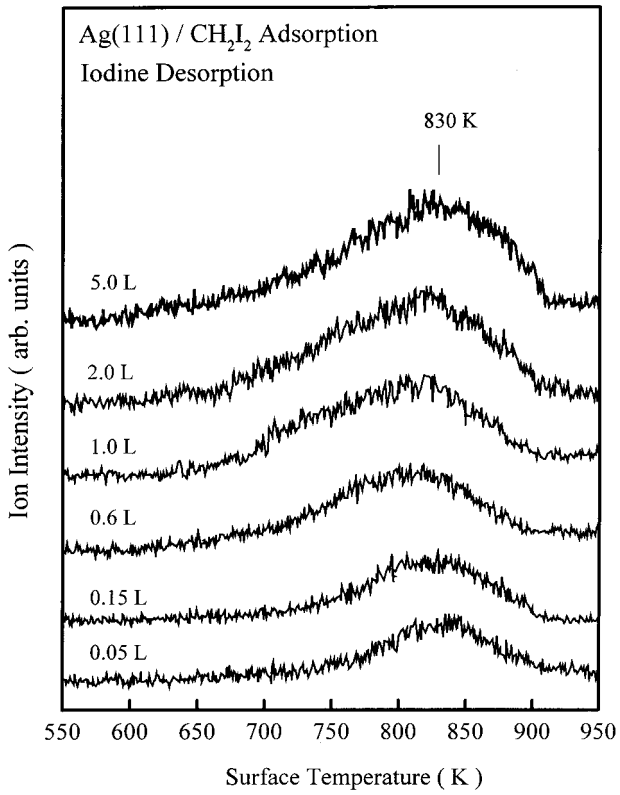

Figure 4. TPR spectra of iodine atoms ($m/e = 127$) from Ag(111) as a function of CH_2I_2 exposure: 0.05, 0.15, 0.6, 1.0, 2.0, and 5.0 L.

coverage up to 1 L and then plateau thereafter. Interestingly, the peak maximum (260 K) does not change with increasing exposure, suggesting first-order kinetics rather than the second-order kinetics expected for a bimolecular recombination reaction. It should be mentioned that the desorption of C_2H_6 formed by the coupling of $CH_{3(ad)}$ from CH_3I/Ag(111) and of C_4H_{10} from C_2H_5I/Ag(111) does not follow second-order desorption kinetics either.[8,9] Even for the recombinative desorption of surface H on Ag(111), fractional-order kinetics instead of second-order kinetics was observed.[25] The deviation of C_2H_4 desorption from the second-order kinetics is probably due to island formation (clustering) of $CH_{2(ad)}$, and slow diffusion of methylene to the periphery of these islands determines the kinetics of ethylene evolution at 260 K. A better understanding of the surface morphology and structure of CH_2/Ag(111) is required in order to account for this behavior.

Auger electron spectroscopy applied after the TPR experiment indicates that no carbon is left behind on the surface. Iodine, however, desorbs above 700 K, as evidenced by the broad desorption feature of $m/e = 127$ in Figure 2. The spectra of atomic iodine desorption for several CH_2I_2 exposures are traced in Figure 4. The integrated areas of I^+ signal saturate at a CH_2I_2 exposure of approximately 1 L with a peak temperature (T_p) near 840 K. With increasing exposure, the T_p decreases, and signal intensity increases. This shift of the iodine desorption feature toward lower temperatures is most likely due to the repulsive interaction within the iodine adlayer. It should be pointed out that CD_2I_2 shows essentially the same chemistry as CH_2I_2.

3.3. The Chemistry of $CH_3I + CH_2I_2$. By using iodomethane (CH_3I) and diiodomethane (CH_2I_2) as precursors, the coadsorption of $CH_{3\,(ad)}$ and $CH_{2\,(ad)}$ on Ag(111) was conducted to investigate the feasibility of methylene insertion into the metal−methyl bond. The experiments were carried out at low surface coverages in order to minimize any effect due to the coadsorbed iodine.

Figure 5 shows TPR spectra of a variety of ions when 0.5 L CH_3I and 0.5 L CH_2I_2 were coadsorbed on Ag(111). On the basis of the chemistry of individual molecules described above, we anticipate the following desorption features, regardless of the possible reaction between CH_3I and CH_2I_2 (if at all). A peak of $m/e = 30$ ($C_2H_6^+$) at 245 K for ethane stemming from CH_3I, and a peak of $m/e = 27$ ($C_2H_3^+$) at 230 K for ethylene resulting from CH_2I_2 along with a minor contribution from ethane cracking, are indeed present. However, the unexpectedly weak $m/e = 30$ signal, as augmented by 3 times in the spectrum, corresponds to an extremely low ethane yield, suggesting that there exist more facile reaction pathways consuming the majority of the methyl moieties on the surface before their dimerization. This argument is strengthened by new desorption features of $m/e = 29$ ($CH_3CH_2^+$), 43 ($CH_3CH_2CH_2^+$), and 58 (CH_3CH_2-$CH_2CH_3^+$) at 225 K. Three-carbon and/or four-carbon hydrocarbon products seem to be formed as a result of the interaction in this mixture of coadsorbed $CH_{3(ad)}$ and $CH_{2(ad)}$. It is known that alkyl groups on the Ag(111) surface undergo carbon−carbon bond-coupling reactions with 100% selectivity to produce alkanes of twice the chain length. If several kinds of alkyl groups coexist on the surface, the self-coupling and cross-coupling among them will make the analysis of products (hydrocarbons) trickier, considering the overlap of masses in their fragmentation patterns. Nevertheless, certain products are still identifiable. In particular, granting that methylene inserts into the Ag−CH_3 bonds to produce *ethyl* groups followed by C−C coupling to yield butane ($CH_3CH_2CH_2CH_3$), the assignment of the $m/e = 58$ signal at 225 K in Figure 5 to the parent ion of butane will be reasonable. To corroborate this proposed insertion

(25) Zhou, X.-L.; White, J. M.; Koel, B. E. *Surf. Sci.* **1989**, *218*, 201.

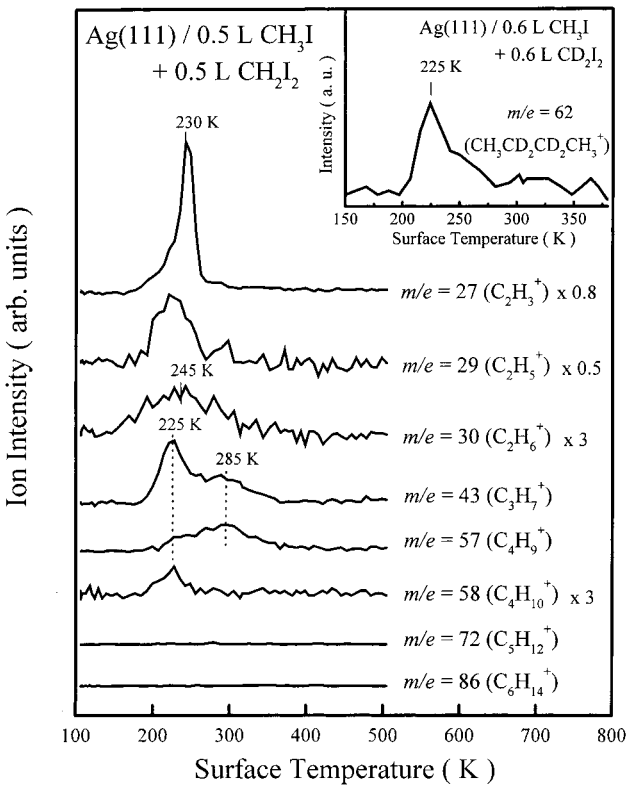

Figure 5. Ions detected in TPR after adsorbing 0.5 L CH_2I_2 followed by 0.5 L of CH_3I on Ag(111) at 180 K. The inset shows the TPR spectrum of $CH_3CD_2CD_2CH_3$ ($m/e = 62$) after the coadsorption of 0.6 L CH_3I and 0.6 L CD_2I_2 at 180 K. The heating rate is 3 K/s.

Table 1. Relative Intensities of Mass Fragment Ions for Ethane, Propane, and Butane

selected ions, m/e	mass spectral data[a]			TPR data[b]		
	ethane	propane	butane	this work[c]	this work[d]	this work[e]
30	100	–	–	56	–	–
29	114	230	263	241	~177	~163
43	–	100	625	100	100	~68
58	–	–	100	5.2	5.2	–

[a] From ref 12. [b] From the integrated peak areas of TPR spectra in the case of 0.5 L CH_3I and 0.5 L CH_2I_2 coadsorbed on the Ag(111) surface. [c] Relative intensities of the selected ion at 225 K. [d] The contribution from ethane is subtracted. [e] The contributions from ethane and butane are subtracted.

mechanism, CH_2I_2 is replaced by CD_2I_2 as the coadsorbate shown in the inset of Figure 5. It is not surprising that the TPR experiments do give rise to butane-d_4 ($m/e = 62$, $CH_3CD_2CD_2$-CH_3^+) evolving at 225 K. Hence, we are confident of the conclusion that the migratory insertion of CH_2 into the Ag–CH_3 bond occurs, generating intermediate ethyl (Ag–CH_2CH_3), which subsequently undergoes self-coupling to produce butane (C_4H_{10}). The direct coupling of ethyl groups on Ag(111) gives a butane desorption peak temperature near 180 K;[9] therefore, the butane evolving with a peak at 225 K must be rate-limited by the methylene insertion step.

Besides C_4H_{10}, there is evidence for the formation of other products at the same temperature, 225 K. To be specific, the observed intensity ratio of $m/e = 58{:}43{:}29$ (the contribution of ethane to $m/e = 29$ is subtracted) does not coincide with the cracking ratio of butane in the mass spectrometer, as shown in Table 1. In our TPR studies, the ratios of $m/e = 43{:}58$ and $29{:}58$ are ~19.2 and ~34.0, respectively. Both ratios are greater than those in a standard mass spectrum for C_4H_{10}, where the ratio of $m/e = 43{:}58$ is ~6.3, and that of $m/e = 29{:}58$ is ~2.6. Therefore, the signals for $m/e = 29$ and 43 in the TPR data must have contributions from other hydrocarbon compounds. When the contribution from C_4H_{10} is subtracted, the ratio of the remaining $m/e = 29{:}43$ becomes ~2.4, which reasonably matches that of propane (see Table 1). A logical inference about the production of propane (C_3H_8) can be attributed to the cross-coupling between the ethyl groups from methylene insertion and the rest of the methyl groups which are not subject to methylene insertion. In light of these processes, very few methyl groups can thus survive after the low-temperature insertion ($CH_2 + CH_3$) and cross-coupling ($C_2H_5 + CH_3$), resulting in the small yield of ethane by methyl self-coupling ($CH_3 + CH_3$).

There are peaks of $m/e = 43$ and 57 at 285 K in Figure 5, representing a different reaction channel, possibly involving multiple CH_2 insertions. But the intensity ratio of $m/e = 57$ (four-carbon) to 43 (three-carbon) is not consistent with any of the cracking ratio of C_4–C_6 alkanes. The origin of these features is not yet clear. Due to the lack of ion signals corresponding to C_5 ($m/e = 72$) and C_6 ($m/e = 86$), the formation of hydrocarbon compounds beyond four-carbon following the coadsorption of CH_3I and CH_2I_2 is not conclusive. The chemistry of $CH_3I + CH_2I_2$ is now summarized in Scheme 1.

Scheme 1

$$CH_3I_{(g)} + CH_2I_{2(g)} \xrightarrow{110\ K} CH_3I_{(ad)} + CH_2I_{2(ad)} \quad \text{Adsorption}$$

$$CH_3I_{(ad)} + CH_2I_{2(ad)} \xrightarrow{<200\ K} CH_{3(ad)} + CH_{2(ad)} + 3I_{(ad)} \quad \text{Dissociation}$$

$$CH_{3(ad)} + CH_{2(ad)} \xrightarrow{\sim 225\ K} CH_3CH_{2(ad)} \quad \text{Methylene Insertion}$$

$$CH_3CH_{2(ad)} + CH_{3(ad)} \rightarrow CH_3CH_2CH_{3(g)} \quad \text{Cross-Coupling}$$

$$CH_3CH_{2(ad)} + CH_3CH_{2(ad)} \rightarrow CH_3(CH_2)_2CH_{3(g)} \quad \text{Self-Coupling}$$

3.4. The Chemistry of CF_3I. There has been a great deal of interest in understanding the reactions of fluorinated alkyl fragments on metal surfaces.[26–35] Again, because the C–I bond scission is facile, the fluorinated alkyl iodides are excellent precursors for investigating the basic chemistry of fluorinated alkyl groups. Their chemistry can be compared to the well-studied reactions of alkyl halides on metals to give insight into the effects of fluorination on reactivity. For example, Paul and Gellman[31] have demonstrated that the activation barriers for alkyl coupling reactions on the Ag(111) surface increase with increasing electron-withdrawing nature of the substituent group-(s). Likewise, it is fundamentally interesting to examine how the methylene insertion reaction could be influenced when $CH_{3(ad)}$ is replaced by $CF_{3(ad)}$. Here, we first probe the independent surface chemistry of CF_3I on Ag(111).

In our TPR/D survey, consistent with the work of White and co-workers,[29,36,37] we found that the thermal chemistry of CF_3I adsorbed on Ag(111) involves molecular desorption below

(26) Jones, R. G.; Singh, N. K. *Vacuum* **1988**, *38*, 213.
(27) Dyer, J. S.; Thiel, P. A. *Surf. Sci.* **1990**, *238*, 169.
(28) Liu, Z.-M.; Zhou, X.-L.; Kiss, J.; White, J. M. *Surf. Sci.* **1993**, *286*, 233.
(29) Castro, M. E.; Pressley, L. A.; Kiss, J.; Pylant, E. D.; Jo, S. K.; Zhou, X.-L.; White, J. M. *J. Phys. Chem.* **1993**, *97*, 8476.
(30) Forbes, J. G.; Gellman, A. J. *J. Am. Chem. Soc.* **1993**, *115*, 6277.
(31) Paul, A.; Gellman, A. J. *J. Am. Chem. Soc.* **1993**, *117*, 9056.
(32) Sun, Z.-J.; Schwaner, A. L.; White, J. M. *Chem. Phys. Lett.* **1994**, *219*, 118.
(33) Armentrout, D. D.; Grassian, V. H. *Langmuir* **1994**, *10*, 2071.
(34) Jensen, M. B.; Thiel, P. A. *J. Am. Chem. Soc.* **1995**, *117*, 438.
(35) Myli, K. B.; Grassian, V. H. *J. Phys. Chem.* **1995**, *99*, 1498; **1995**, *99*, 5581.

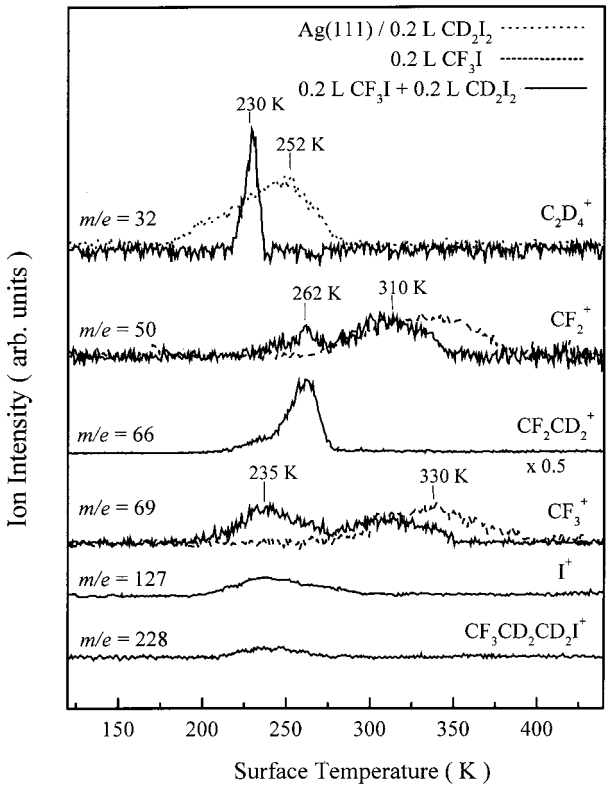

Figure 6. TPR spectra from CD_2I_2, CF_3I, and $CD_2I_2 + CF_3I$. Dotted and dashed curves show the TPR spectra following separate adsorption of 0.2 L CD_2I_2 and 0.2 L CF_3I, respectively; solid curves show the spectra when 0.2 L CD_2I_2 and 0.2 L CF_3I are coadsorbed on Ag(111) at 180 K. It should be pointed out that the results were essentially the same as the order of the coadsorption was reversed.

150 K and the dissociation of the C−I bond to form $CF_{3(ad)}$ and $I_{(ad)}$. There is no C−F bond cleavage upon further heating. Unlike $CH_{3(ad)}$, trifluromethyl groups do not self-couple to form C_2F_6 but, instead, liberate as radicals near 320 K. Because F is larger than H in size and is more negatively charged, the lateral repulsion among adsorbed $CF_{3(ad)}$ species thus inhibits their proximity, disfavoring the C_2F_6 formation. Applying Paul and Gellman's proposition that the transition state for alkyl coupling reactions is *electron deficient*,[31] it is conceivable that, when hydrogen is substituted by the more electronegative fluorine, the transition state would be destabilized, leading to an increase of the activation barrier. Consequently, the coupling reaction rate for $CF_{3(ad)}$ becomes slow enough that it is preceded by the ejection of CF_3 radicals. This theory is confirmed in the TPR experiments because the 320 K representing CF_3 radical ejection from Ag(111) places a lower limit for the $CF_{3(ad)}$ self-coupling reaction, ensuring that the coupling temperature for $CF_{3(ad)}$ is higher than that for $CH_{3(ad)}$ (∼255 K, see section 3.1). Finally, the atomic iodine desorbs at approximately 830 K. There are no desorption products other than CF_3I, CF_3 radicals, and atomic iodine.

3.5. The Chemistry of $CF_3I + CD_2I_2$. Using $CD_{2(ad)}$ as the carbon chain growth species and $CF_{3(ad)}$ as the target for insertion, we now study the CD_2 migratory insertion into the Ag−CF_3 bond in a coadsorbed mixture of CF_3I and CD_2I_2. Figure 6 shows the TPR spectra for $m/e = 32$, 50, 66, 69, 127, and 228 ions. The dashed and dotted curves are the TPR spectra obtained when 0.2 L CF_3I and 0.2 L CD_2I_2 are adsorbed individually, while the solid curves are the spectra for the coadsorbed mixture. First, the dotted curve of $m/e = 32$ with the peak maximum at 252 K represents ethylene-d_4 (C_2D_4) evolution from the separate reaction of CD_2I_2. The dashed curves of $m/e = 50$ (CF_2^+, the most abundant fragment ion of the CF_3 radical in the mass spectrometer) and 69 (CF_3^+) at 330 K indicate the CF_3 radical ejection known in the CF_3I chemistry. The comparison of the dotted to the solid curve of $m/e = 32$ ($C_2D_4^+$) in Figure 6 illustrates that, in the presence of coadsorbed CF_3I, the intensity of C_2D_4 diminishes, and the peak temperature shifts to 230 K. Similarly, the contrast between the dashed and solid curves suggests that, in the presence of coadsorbed CD_2I_2, the intensities of both $m/e = 69$ and 50 decrease, and the peak maximum temperature shifts to 310 K. The reduction in the yields of C_2D_4 and CF_3 radicals is accompanied by the emergence of new desorption features of $m/e = 50$ and 66 at 262 K, as well as new peaks of $m/e = 69$, 127, and 228 at 235 K, as shown in Figure 6. These new TPR peaks above 200 K undoubtedly stem from the interaction between $CF_{3(ad)}$ and $CD_{2(ad)}$. First, the heaviest ion detected at 262 K was $C_2D_2F_2^+$ ($m/e = 66$), which is also the molecular weight for $CF_2{=}CD_2$. The fragmentation pattern of the $CF_2{=}CD_2$ and the ratio of $m/e = 50$ (CF_2^+) to $m/e = 66$ ($CF_2CD_2^+$) based on their integrated areas are found to be consistent with the standard mass spectral pattern in the Wiley/NBS handbook.[12] Therefore, the mechanism shown in Scheme 2 is proposed to account for our TPR observations.

Scheme 2

$$CF_3I_{(g)} + CD_2I_{2(g)} \xrightarrow{110\ K} CF_3I_{(ad)} + CD_2I_{2(ad)} \qquad \text{Adsorption}$$

$$CF_3I_{(ad)} + CD_2I_{2(ad)} \xrightarrow{<200\ K} CF_{3(ad)} + CD_{2(ad)} + 3I_{(ad)} \qquad \text{Dissociation}$$

$$CF_{3(ad)} + CD_{2(ad)} \rightarrow CF_3CD_{2(ad)} \qquad \text{Methylene Insertion}$$

$$CF_3CD_{2(ad)} \xrightarrow{\sim 262\ K} CF_2{=}CD_{2(g)} + F_{(ad)} \qquad \beta\text{-Fluoride Elimination}$$

Briefly, trifluoromethyl (CF_3) and methylene-d_2 (CD_2) moieties are generated on Ag(111) by the dissociative adsorption of CF_3I and CD_2I_2. The $CD_{2(ad)}$ group is inserted into the Ag−CF_3 bond to form $CF_3CD_{2(ad)}$, which then undergoes β-fluoride elimination to evolve $CF_2{=}CD_2$ at 262 K. Paul and Gellman[38] found that the adsorbed $CF_3CH_{2(ad)}$, generated directly on the Ag(111) surface by thermally rupturing the C−I bond in adsorbed CF_3CH_2I, indeed loses one fluorine at the β carbon position, to afford $CF_2{=}CH_2$ at ∼250 K. Since the situations of $CF_{3(ad)} + CH_{2(ad)}$ ($CF_{3(ad)} + CD_{2(ad)}$) and $CF_3CH_{2(ad)}$ lead to identical end products, the insertion of methylene into the Ag−CF_3 bond is strongly inferred.[7] To test this argument further, Figure 7 (top panel) shows the evolution of $CF_2{=}CH_2$ in TPR as a result of $CH_{2(ad)} + Ag{-}CF_3 \rightarrow Ag{-}CH_2CF_3 \rightarrow CH_2{=}CF_{2(g)} + F_{(ad)}$ (methylene insertion/β-elimination) after the coadsorption of 1.0 L CH_2I_2 and 0.3 L CF_3I. In contrast, Figure 7 (bottom panel) shows the evolution of $CF_2{=}CH_2$ in TPR as well, however, as a direct consequence of β-fluoride elimination from $CF_3CH_{2(ad)}$ exclusively generated by the dissociative adsorption of 0.1 L CF_3CH_2I. The fact that $CF_3I + CH_2I_2$ and CF_3CH_2I essentially result in the same desorption temperature of $CF_2{=}CH_2$ suggests that β-fluoride elimination is the rate-determining step in Scheme 2, instead of the methylene insertion.

(36) Szabo, A.; Converse, S. E.; Whaley, S. R.; White, J. M. *Surf. Sci.* **1996**, *364*, 345.
(37) Junker, K. H.; Sun, Z.-J.; Scoggins, T. B.; White, J. M. *J. Chem. Phys.* **1996**, *104*, 3788.
(38) Paul, A.; Gellman, A. J. *Langmuir* **1995**, *11*, 4433.

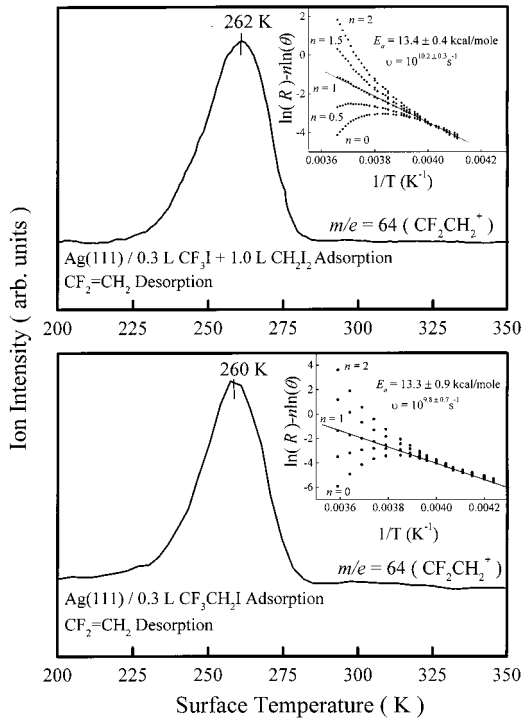

Figure 7. (Top) Thermal evolution of 1,1-difluoroethylene (as monitored by $m/e = 64$, $CF_2CH_2^+$) after coadsorption of 0.3 L CF_3I and 1.0 L CH_2I_2 on Ag(111) at 180 K. Inset: The data are plotted as $\ln(R) - n \ln(\theta_{CF_3CH_2})$ vs $1/T$ for $n = 0$, 0.5, 1, 1.5, and 2 in order to determine the best value for n (the reaction order). The line indicates the best fit to $n = 1$, and the slope of the line gives the activation barrier $E_a = 13.4 \pm 0.4$ kcal/mol; the intercept gives the preexponential factor $\nu = 10^{10.2 \pm 0.3}$ s^{-1}. (Bottom) Rate of $CF_2{=}CH_2$ evolution as a function of surface temperature after the exposure of 0.3 L CF_3CH_2I on Ag(111) at 110 K. The heating rate is 2 K/s. Inset: The $\ln(R) - n \ln(\theta_{CF_3CH_2})$ vs $1/T$ for $n = 0$, 0.5, 1, 1.5, and 2 plot. First-order kinetics ($n = 1$) best fit the data. The slope of the line gives the activation barrier (E_a) for the β-fluoride elimination reaction.

We adopt a method described in detail by Parker et al.[39] to calculate the thermal activation energy, E_a. In both insets of Figure 7, we plot out $\ln(R) - n \ln(\theta_{CF_3CH_2})$ vs $1/T$ for $n = 0$, 0.5, 1, 1.5, and 2. Here, R is proportional to the height of ion intensity at any specific temperature T of the TPR curve, $\theta_{CF_3CH_2}$ is calculated from the remaining integrated partial TPR peak areas (by integration from T to infinity), and n stands for the reaction order. From the best linear fit and the slopes, $n = 1$ and $E_a = 13.4 \pm 0.4$ ($CF_3I + CH_2I_2$) and 13.3 ± 0.9 kcal/mol (CF_3CH_2I), respectively. Clearly, the values of these kinetic parameters are almost identical in both cases.

Attention is now shifted to the other new desorption features appearing at 235 K as a result of the coadsorption of CF_3I and CD_2I_2 in Figure 6. The solid curves of $m/e = 69$, 127, and 228, having the same peak shape and maxima, are attributable to a new product containing iodine. The existence of iodine in this compound suggests that the carbon−iodine bond is re-formed. The heaviest ion detected ($m/e = 228$) happens to be the molecular weight of $CF_3CD_2CD_2I$. By checking the fragmentation pattern of the $CF_3CH_2CH_2I$ molecule in our mass spectrometer, the cracking ratio of I^+ to $CF_3CH_2CH_2^+$ is 1.2:1, consistent with the intensity ratio of $m/e = 127$ (I^+) to 101 ($CF_3CD_2CD_2^+$). Hence, we argue that the new compound formed at 235 K is $CF_3CD_2CD_2I$ when CF_3I and CD_2I_2 are coadsorbed, and the mechanism must involve two consecutive CD_2 insertions, terminated by the recombination of a 1,1,1-trifluoropropyl group ($CF_3CD_2CD_2$) and iodine, as depicted in Scheme 3.

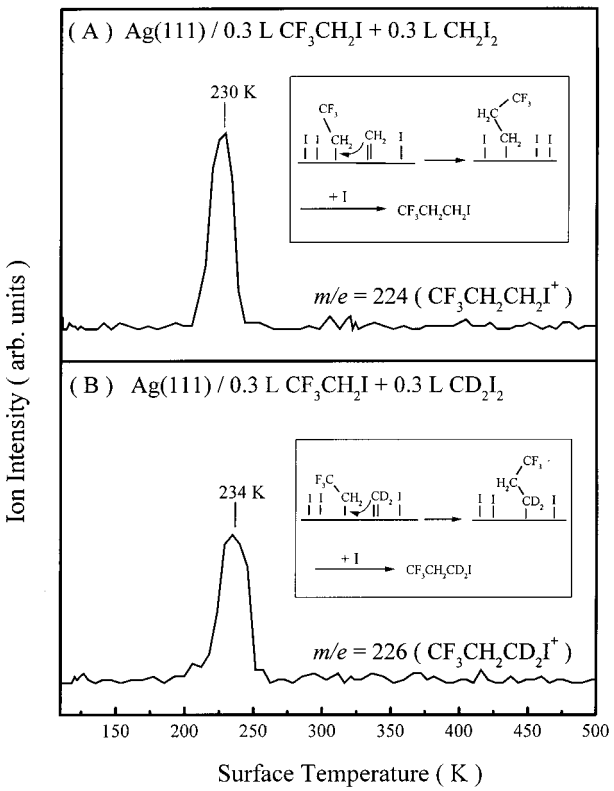

Figure 8. TPR spectra of (A) 1,1,1-trifluoropropyl iodide (CF_3CH_2-CH_2I^+, $m/e = 224$) and (B) 1,1,1-trifluoropropyl iodide-3-d_2 (CF_3CH_2-CD_2I^+, $m/e = 226$) formed by reacting CF_3I with CH_2I_2 and CD_2I_2, respectively. The heating rate is 3 K/s.

Scheme 3

$$CF_{3(ad)} + CD_{2(ad)} \rightarrow CF_3CD_{2(ad)} \qquad \text{First Methylene Insertion}$$

$$CF_3CD_{2(ad)} + CD_{2(ad)} \xrightarrow{<235\ K} CF_3CD_2CD_{2(ad)} \qquad \text{Second Methylene Insertion}$$

$$CF_3CD_2CD_{2(ad)} + I_{(ad)} \xrightarrow{\sim 235\ K} CF_3CD_2CD_2I_{(g)} \qquad \text{R−I Recombination}$$

Methylene insertion into perfluoroethyl (CF_3CH_2) groups to form perfluoropropyl ($CF_3CH_2CH_2$) groups, followed by the recombination with surface iodine, i.e., the second and third steps in Scheme 3, can be modeled by TPR experiments using the coadsorption of CF_3CH_2I and CH_2I_2 (CD_2I_2). In Figure 8, the reaction of $CF_3CH_2I + CH_2I_2$ does evolve $CF_3CH_2CH_2I$ (as monitored by $m/e = 224$, $CF_3CH_2CH_2I^+$, top panel) from Ag(111), while the reaction with CD_2I_2 produces $CF_3CH_2CD_2I$ (as monitored by $m/e = 226$, $CF_3CH_2CD_2I^+$, bottom panel). The desorption peak temperature (∼230 K) also matches that in the case initiated from $CF_3I + CD_2I_2$. These results confirm that the second methylene insertion into the Ag−CH_2CF_3 bond to form propyl species is plausible, and the propagation of the carbon chain is subsequently terminated by the recombination with surface iodine, as depicted in the insets. However, it is legitimate to ask why the fate of $CF_3CD_2CD_{2(ad)}$ generated by two sequential insertions after the coadsorption of CF_3I and CD_2I_2 is not the C−C coupling reaction yielding $CF_3CD_2CD_2$-$CD_2CD_2CF_3$; instead it recombines with $I_{(ad)}$ to form CF_3CD_2-CD_2I. The difference could be caused by the high coverage of iodine when CF_3I and CD_2I_2 are coadsorbed on Ag(111). We will study this issue in detail in the next section. In addition to the mechanism proposed in Scheme 3, the three-carbon and

(39) Parker, D. H.; Jones, M. E.; Koel, B. E. *Surf. Sci.* **1990**, *223*, 65.

iodine-containing product, $CF_3CD_2CD_2I$, could be due to coupling of $CF_3CD_{2(ad)}$ with $CD_2I_{(ad)}$ (from partial dissociation of CD_2I_2). However, this alternative pathway is more difficult to verify. In contrast, the pathway shown in Scheme 3 can be substantiated by experiments using an iodine-precovered surface. This point will be discussed specifically in the next section.

4. Discussion

4.1. Mechanism and Kinetics: Insertion, Coupling, and β-Elimination. The methylene insertion into the metal−carbon bond has been clearly elucidated in the two systems studied, $CH_{2(ad)} + CH_{3(ad)}$ and $CH_{2(ad)} + CF_{3(ad)}$. The chemical evidence based on TPR experiments supports the mechanisms proposed in Schemes 1−3, although direct spectroscopic evidence for the surface intermediates, such as the high-resolution electron energy loss spectra (HREELS) of $CH_3CH_{2(ad)}$ or $CF_3CH_{2(ad)}$, would be desirable. Nevertheless, the conversion of two coadsorbed C_1 species into butane (a C_4 alkane) in the case of $CH_{2(ad)} + CH_{3(ad)}$ and the conversion into difluoroethylene (CF_2═CH_2, a C_2 olefin) in the case of $CH_{2(ad)} + CF_{3(ad)}$ prove not only that the carbon−carbon bonds are formed but also that the chain growth must rely on the CH_2 insertion reaction. Two aspects of the insertion reaction kinetics will be discussed.

(1) The fact that butane is formed at 225 K reflects the relative rates of *CH_2CH_3 coupling*, *CH_2 insertion*, and *β-elimination*. Using C_2H_5I as a precursor, Zhou and White[9] have shown that ethyl coupling evolves butane with desorption temperatures in the range of 175−220 K. In contrast, the 225 K butane desorption temperature in the TPR of $CH_{2(ad)} + CH_{3(ad)}$ indicates that *the CH_2 insertion step is slower than the ethyl coupling step and is the rate-determining step (rds) in Scheme 1*. β-Hydride elimination is the most favorable alkyl decomposition pathway on surfaces. This preference has been established for ethyl groups on single-crystal surfaces of Al,[40] Fe,[41] Ni,[42] Pd,[43] Pt,[44−47] Cu,[48−50] and Au.[51,52] Interestingly, on Ag, alkyl groups couple with 100% efficiency,[8−11] perhaps because the low affinity of silver for hydrogen inhibits any hydride elimination steps (kinetically disfavored). Therefore, *β-elimination is too slow to compete with ethyl coupling as the termination step after the CH_2 insertion*. The relative rates are *ethyl coupling > CH_2 insertion* (rds) > *methyl coupling > β-elimination*.

In the case of $CH_{2(ad)} + CF_{3(ad)}$, the fact that CH_2═CF_2 is formed at 262 K also reflects the relative rates of *CH_2CF_3 coupling*, *CH_2 insertion*, and *β-elimination*. As opposed to its hydrocarbon counterpart, CH_2CF_3 (1,1,1-trifluoroethyl) can lose a fluorine atom from the second carbon (the β position) to release a free perfluoroalkene.[38] In fact, when the adsorbed alkyl group is fluorinated at either the α-carbon or β-carbon position, the usual coupling reaction pathway is blocked. From a different perspective, the addition of electron-withdrawing substituents (F and CF_3) increases the activation barriers to the point that CF_3 radical ejection (complete fluorination of the methyl group) and β-fluoride elimination (substitution of the methyl group with one CF_3) replace coupling as the dominant (most facile) pathways on the Ag(111) surface. We can conclude that *CH_2CF_3 coupling is the slowest* one among the three elementary steps discussed here. Both $CH_{2(ad)} + CF_{3(ad)}$ (insertion/β-elimination) and $CH_2CF_{3(ad)}$ (β-elimination) give rise to CH_2═CF_2, indicating that *β-elimination is the termination step after the CH_2 insertion*. The kinetic resemblance based on the TPR features of CH_2═CF_2 (same shape, peak temperature, and activation energy) reveals that *β-fluoride elimination controls the formation rate*. According to our kinetic analysis, the first-order behavior (n = 1) is consistent with the rate-limiting step being an unimolecular process; therefore, β-elimination (unimolecular) is more plausible than CH_2 insertion into the Ag−CF_3 bond (bimolecular) as the rate-determining step in Scheme 2. $CF_3CH_2CH_2I$, attributed to *two sequential methylene insertions* followed by recombination with surface iodine in Scheme 3, evolves at a lower temperature (235 K) than β-elimination (262 K), ensuring that the CH_2 insertion step is, indeed, more facile. Hence, the relative rates are *CH_2 insertion > β-elimination* (rds) > *CF_3CH_2 coupling*. As a matter of fact, the desorption temperature of $CF_3CH_2CH_2I$ (235 K) places a kinetic upper limit for the insertion of CH_2 into the Ag−CF_3 bond. Altogether, we can establish that the insertion of CH_2 into Ag−CH_3 occurs at about 225 K,

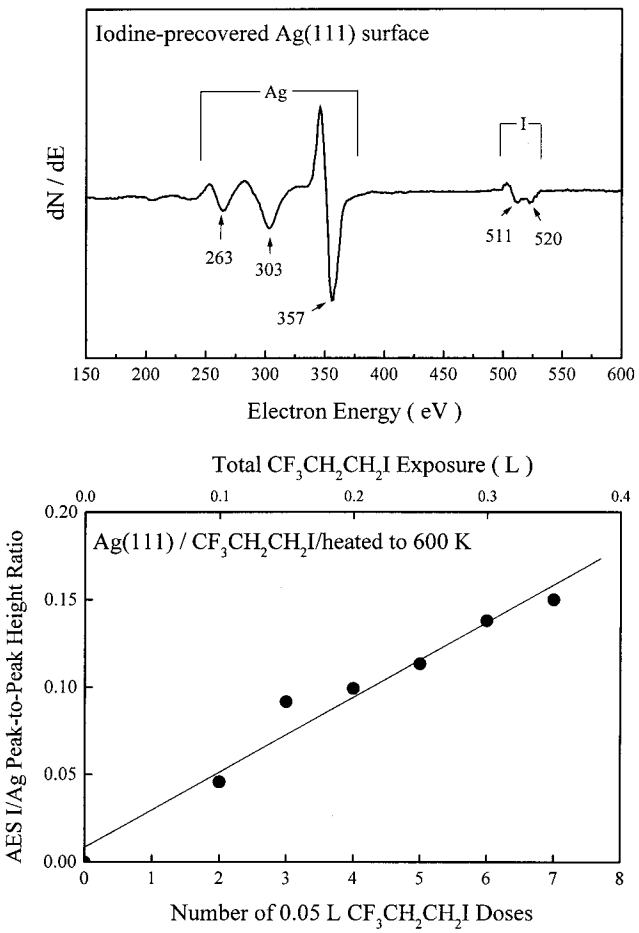

Figure 9. Uptake of surface iodine as a function of the number of 0.05 L $CF_3CH_2CH_2I$ doses (bottom). The AES measurements were performed after flashing the surface to 600 K (top), and the atomic I/Ag ratios were obtained by measuring the peak-to-peak heights, corrected by AES sensitivity factors of the MNN transition of iodine at 520 eV and that of silver at 357 eV.

(40) Bent, B. E.; Nuzzo, R. G.; Zegarski, B. R.; Dubois, L. H. *J. Am. Chem. Soc.* **1991**, *113*, 1137.
(41) Burke, M. L.; Madix, R. J. *J. Am. Chem. Soc.* **1992**, *114*, 2780.
(42) Tjandra, S.; Zaera, F. *Surf. Sci.* **1993**, *289*, 255.
(43) Kovaćs, I.; Solymosi, F. *J. Phys. Chem.* **1993**, *97*, 11056.
(44) Zaera, F. *Surf. Sci.* **1989**, *219*, 453.
(45) Zaera, F. *J. Phys. Chem.* **1990**, *94*, 8350.
(46) Zaera, F. *J. Am. Chem. Soc*. **1989**, *111*, 8744.
(47) Lloyd, K. G.; Campion, A.; White, J. M. *Catal. Lett.* **1989**, *2*, 105.
(48) Lin, J.-L.; Bent, B. E. *J. Am. Chem. Soc.* **1993**, *115*, 6943.
(49) Jenks, C. J.; Xi, M.; Yang, M. X.; Bent, B. E. *J. Phys. Chem.* **1994**, *98*, 2152.
(50) Jenks, C. J.; Chiang, C.-M.; Bent, B. E. *J. Am. Chem. Soc*. **1991**, *113*, 6308.
(51) Paul, A.; Yang, M. X.; Bent, B. E. *Surf. Sci.* **1993**, *297*, 327.
(52) Yang, M. X.; Jo, S. K.; Paul, A.; Avila, L.; Bent, B. E.; Nishikida, K. *Surf. Sci.* **1995**, *325*, 102.

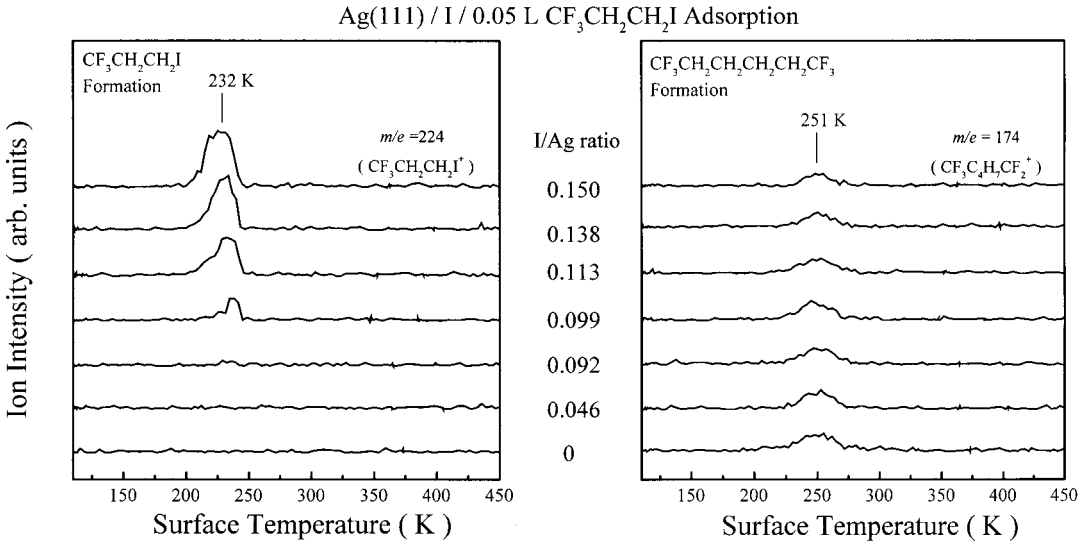

Figure 10. Evolution of $CF_3CH_2CH_2I$ (left panel) and $CF_3CH_2CH_2CH_2CH_2CF_3$ (right panel) after 0.05 L exposure of $CF_3CH_2CH_2I$ on various iodine-precovered Ag(111) surfaces at 110 K. These results show that $CF_3CH_2CH_2CH_2CH_2CF_3$ (C−C coupling product) is inhibited and $CF_3CH_2CH_2I$ (C−I recombination product) is promoted as a function of increasing surface iodine coverage.

and the insertion into Ag−CF_3 takes place below 235 K. Nevertheless, a definitive rate comparison between these two processes is somewhat formidable.

(2) Why are there two consecutive insertions in $CF_{3(ad)}$ + $CH_{2(ad)}$, but only one in $CH_{3(ad)}$ + $CH_{2(ad)}$? In Scheme 1, the chain growth by *methylene insertion* competes with the chain termination by *alkyl coupling*. The slower rate of the chain-propagating step relative to the termination step is the primary reason for the lack of the second and even more CH_2 insertions. In Scheme 2, the situation is reversed, where the chain growth by methylene insertion has a faster rate than the chain termination by *β-fluoride elimination*. However, when the chain is built up to three-carbon to give rise to $CF_3CH_2CH_{2(ad)}$, a more efficient termination step (the recombination with iodine) comes in to compete, yielding $CF_3CH_2CH_2I_{(g)}$ as the end product, shown in Scheme 3.

4.2. The Effect of Coadsorbed Iodine. We have mentioned that $CF_3CH_2CH_{2(ad)}$ recombines with surface iodine when it is formed after two sequential CH_2 insertions following the coadsorption of CF_3I and CH_2I_2. This is unlike the adsorbed $CF_3CH_2CH_{2(ad)}$ generated independently on the Ag(111) surface by thermal dissociation of the C−I bond in $CF_3CH_2CH_2I$ (see section 3.5), where the C−C coupling reaction is the primary pathway. In fact, Paul and Gellman[38] have pointed out that the usual coupling reaction is observed when the adsorbed alkyl group is fluorinated beyond the β-carbon position (F is at the γ-carbon for $CF_3CH_2CH_2$). On the basis of simple stoichiometry, there exist three iodine atoms in each coadsorbed experiment (CH_2I_2 + CF_3I), as opposed to only one when using $CF_3CD_2CD_2I$ as the sole precursor. We believe that the relatively large concentrations of surface iodine result in the shift of reaction pathway. In other words, the high iodine coverages enhance the chance of recombination between $CF_3CH_2CH_{2(ad)}$ with $I_{(ad)}$ rather than the self-coupling of $CF_3CH_2CH_{2(ad)}$.

To understand the role of iodine, we studied the reaction of $CF_3CH_2CH_2I$ on an iodine-precovered Ag(111) surface. Figure 9 shows how $I_{(ad)}$ is accumulated using repeated 0.05 L doses of $CF_3CH_2CH_2I$, followed by heating the surface to 600 K to eliminate only the adsorbed hydrofluorocarbon species. Auger electron spectra taken after each aforementioned procedure (top of Figure 9) reveal that all carbon and fluorine could be removed from the surface by the volatile products discussed before. Iodine left behind on the surface could only be removed by annealing to 950 K. As shown in the bottom of Figure 9, the I(MNN)/Ag(MNN) values, estimated by taking the ratio of peak-to-peak heights (measured in the d$N(E)$/dE mode) corrected by the Auger sensitivity factors, are plotted as a function of the total number of 0.05 L $CF_3CH_2CH_2I$ doses. The I/Ag ratios increase fairly linearly with exposure. The uptake does not reach saturation with a total accumulated exposure of 0.35 L $CF_3CH_2CH_2I$ (seven doses), and an I/Ag ratio of ∼0.15 is attained.

Figure 10 juxtaposes the TPR spectra of $CF_3CH_2CH_2I$ (as monitored by m/e = 224, $CF_3CH_2CH_2I^+$) and $CF_3CH_2CH_2CH_2CH_2CF_3$ (as monitored by m/e = 174, $CF_3C_4H_7CF_2^+$) after dosing 0.05 L $CF_3CH_2CH_2I$ on the Ag(111) surface which was already precovered by various amounts of iodine (indicated by the I/Ag ratios). At low iodine coverages (I/Ag < 0.092), the desorption peak of $CF_3CH_2CH_2CH_2CH_2CF_3$ appears at ∼250 K, and the yields remain nearly constant at this stage. Meanwhile, the evolution of $CF_3CH_2CH_2I$ is not observed. When I/Ag reaches ∼0.1, there is a little change in the $CF_3CH_2CH_2CH_2CH_2CF_3$ peak area; however, a peak for $CF_3CH_2CH_2I$ now emerges at ∼230 K. When I/Ag ratios are higher than 0.1, the yields of $CF_3CH_2CH_2CH_2CH_2CF_3$ proceed to decrease, and the yields of $CF_3CH_2CH_2I$ increase concomitantly. These trends are illustrated in Figure 11 using the integrated TPR peak areas of $CF_3CH_2CH_2I$ (solid squares) and $CF_3CH_2CH_2CH_2CH_2CF_3$ (solid circles) plotted as a function of the Auger I/Ag ratio. Clearly, with a high coverage of iodine on the Ag(111) surface, there is a crossover from the C−C coupling reaction of $CF_3CH_2CH_{2(ad)}$ to the recombination of $CF_3CH_2CH_{2(ad)}$ with $I_{(ad)}$, forming $CF_3CH_2CH_2I$. The correlation between coadsorbed iodine and its effect on the switching of reaction pathways for $CF_3CH_2CH_{2(ad)}$ on Ag(111) is established. In light of this information, we speculate that sequential methylene insertions on Ag surfaces will occur more repeatedly to produce higher (>C_4) hydrocarbons, provided that both $CF_{3(ad)}$ and $CH_{2(ad)}$ can be generated without the coadsorption of iodine. Experiments utilizing pyrolysis of *perfluoro*azomethane ($CF_3N_2CF_3$) and diazomethane (CH_2N_2) as the source of CF_3 and CH_2 species are underway.

4.3. Comparison with Other Metals. The "pressure gap" has been blamed for the difficulties in studying catalytic bond synthesis reactions under UHV, since the high reactivity of atomically clean surfaces and low concentrations of the surface intermediates favor bond dissociation (unimolecular) over bond

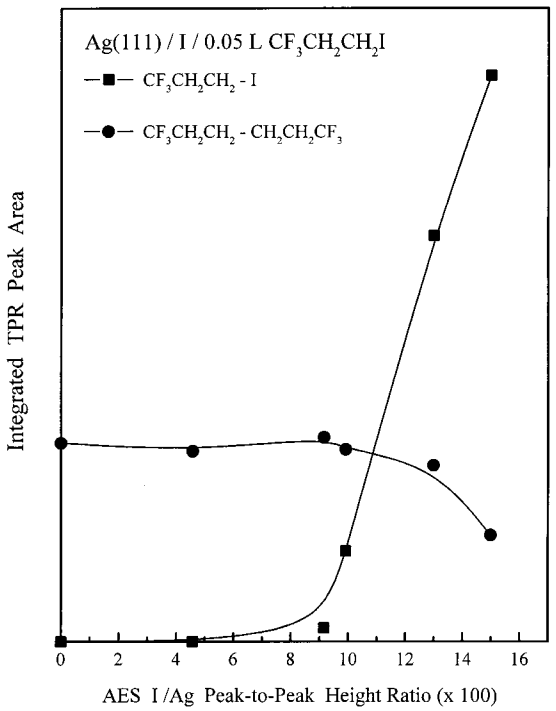

Figure 11. Yields of the $CF_3CH_2CH_2CH_2CH_2CF_3$ (as monitored by the TPR peak areas of $CF_3CH_2CH_2CH_2CHCF_2^+$, $m/e = 174$, in Figure 10) and $CF_3CH_2CH_2I$ (as monitored by the TPR peak areas of $CF_3CH_2CH_2I^+$, $m/e = 224$, in Figure 10) as a function of atomic I/Ag ratio.

formation (bimolecular). The reason that we are able to study the methylene insertion reaction (a typical C−C bond formation reaction) is largely due to the use of the Ag(111) surface. First, Ag(111) is relatively inert toward C−H and C−F activation of methyl, perfluoromethyl, and methylene under vacuum conditions, whereas dehydrogenation reactions occur preferentially on other metals, such as Ni,[53] W,[54] Fe,[55] Pd,[56] Co,[57] Pt,[44,58] and even Cu.[59] When two C_1 fragments are coadsorbed on Ag(111), complication from a third species (due to unimolecular decomposition of the incipient C_1 species) can be completely ruled out, and the chemical effects caused by the bimolecular interaction can be identified without any ambiguity. Second, Ag(111) has been experimentally proven to facilitate C−C bond formation with 100% selectivity with respect to alkyl fragments. Besides, extended Hückel calculations by Hoffmann and coworkers[60] also indicate an increase of the coupling rate (decrease of the reaction barrier) for $CH_2 + CH_3$ on model surfaces as the metal is changed, moving from the left to the right side of the Periodic Table. No wonder copper and silver are the only two metals to date that have been reported to catalyze carbon chain propagation via methylene insertion.[7,61] On Cu(110), the thermal interaction of coadsorbed mixtures of methyl and methylene groups yields *ethylene*, which is produced by β-hydride elimination from the ethyl moieties resulting from CH_2 insertion into the Cu−CH_3 bond.[59] However, this proof of insertion is somewhat implicit considering the self-coupling of methylene, which generates ethylene at similar temperatures as well. We recall that, on Ag(111), *butane* desorption is the evidence for methylene insertion in the case of $CH_2 + CH_3$, while *1,1-difluoroethylene* is our corroboration of CH_2 insertion, changing the target from CH_3 to CF_3. As a comparison, a simpler and clearer demonstration is provided by the Ag(111) surface.

As far as the relative rates of methylene insertion on Ag and Cu are concerned, we have found that the insertion reaction occurs with about a 35 K higher peak temperature on Cu(100) (as measured by evolution of ethylene-d_2 at 260 K when CH_2I_2 and CD_3I are coadsorbed[61]) than on Ag(111) (as measured by evolution of butane at 225 K when CH_2I_2 and CH_3I are coadsorbed). The contrast is more dramatic with a 60 K difference on corrugated Cu(110), but data are not available on Cu(111). As an estimate, reaction rates increase by an order of magnitude for every 20−30 K increment in temperature. For example, a first-order reaction whose TPR peak is 250 K will have an activation energy of ∼15 kcal/mol for a typical preexponential factor of 10^{13} s^{-1}. Increasing the temperature to 270 K enhances the rate by an order of magnitude. Therefore, the insertion rate is generally faster on silver than on copper.

5. Conclusions

We report the reaction pathways of methyl iodide (CH_3I) and trifluoromethyl iodide (CF_3I) with and without the coadsorbed methylene iodide (CH_2I_2 or CD_2I_2) on Ag(111) under ultrahigh-vacuum conditions. The results have suggested that CH_3I, CF_3I, and CH_2I_2 (CD_2I_2) are effective precursors for generating surface-bound CH_3, CF_3, and CH_2 (CD_2) moieties, respectively. The chemistry of these species adsorbed alone on the surface can be summarized as follows: (1) methyl undergoes a self-coupling reaction to form ethane, (2) methylene is dimerized to form ethylene, and (3) trifluoromethyl desorbs as a radical. In contrast, TPR spectra taken after the coadsorption of CH_3I and CH_2I_2 indicate bimolecular interaction between $CH_{3(ad)}$ and $CH_{2(ad)}$. Ethyl groups are formed by methylene insertion into the Ag−CH_3 bond, and the subsequent self- and/or cross-coupling reactions of alkyl groups on the surface produce propane and butane. These volatile products are all evolved from the surface between 200 and 300 K. To support the methylene insertion mechanism using a different approach, the interaction of CF_3 and CH_2 coadsorbed on Ag(111) is investigated. Again, CH_2 is found to insert into the Ag−CF_3 bond; however, this is followed by β-fluoride elimination to produce 1,1-difluoroethylene (CF_2═CH_2) at 260 K. Two sequential methylene insertions are invoked by the evolution of 1,1,1-trifluoropropyl iodide ($CF_3CH_2CH_2I$) at 235 K due to the recombination of $CF_3CH_2CH_{2(ad)}$ and surface iodine. These results provide a distinct demonstration of the migratory insertion of methylene into metal−carbon bonds and useful kinetic information, which are crucial to the understanding of carbon−carbon bond-forming steps in catalytic polymerization processes of the Fischer−Tropsch synthesis.

Acknowledgment. The late Professor Brian Bent inspired this research with his everlasting influences. The financial support of the National Science Council of the Republic of China (Grants Nos. 87-2732-M-110-001 and 87-2113-M-110-008) and National Sun Yat-Sen University is gratefully acknowledged.

JA983164C

(53) Zhou, X.-L.; White, J. M. *Surf. Sci.* **1988**, *194*, 438.
(54) Zhou, X.-L.; Yoon, C.; White, J. M. *Surf. Sci.* **1988**, *206*, 379.
(55) Benzinger, J. B.; Madix, R. J. *J. Catal.* **1980**, *65*, 49.
(56) Solymosi, F.; Revesz, K. *J. Am. Chem. Soc.* **1991**, *113*, 9145.
(57) Steinbach, R.; Kiss, J.; Krall, R. *Surf. Sci.* **1985**, *157*, 401.
(58) Henderson, M. A.; Mitchell, G. E.; White, J. M. *Surf. Sci.* **1987**, *184*, L325.
(59) Chiang, C.-M.; Wentzlaff, T. H.; Bent, B. E. *J. Phys. Chem.* **1992**, *96*, 1836.
(60) Zheng, C.; Apeloig, Y.; Hoffmann, R. *J. Am. Chem. Soc*. **1988**, *110*, 749.
(61) Lin, J.-L.; Chiang, C.-M.; Jenks, C. J.; Yang, M. X.; Wentzlaff, T. H.; Bent, B. E. *J. Catal.* **1994**, *147*, 250.